

A New WDS Spectrometer for Valence Electron Spectroscopy Based on Electron Microscopy

Masami Terauchi[†], Hideyuki Takahashi^{††}, Nobuo Handa^{††},
Takanori Murano^{††}, Masato Koike^{†††}, Tetsuya Kawachi^{†††}, Takashi
Imazono^{†††}, Masaru Koeda^{††††}, Tetsuya Nagano^{††††}, Hiroyuki
Sasai^{††††}, Yuki Oue^{††††}, Zeno Yonezawa^{††††} and Satoshi Kuramoto^{††††}

[†] IMRAM, Tohoku University

^{††} EO Peripheral Component Business Unit, JEOL Ltd.

^{†††} Quantum Beam Science Directorate, Japan Atomic Energy Agency

^{††††} Device Department, SHIMADZU Corp.

A new WDS spectrometer for a transmission electron microscope has been constructed. This spectrometer can cover an energy region from 50 eV to 3800 eV by using four aberration-corrected gratings for flat-field optics. By using a newly designed and manufactured grating of JS50XL for 50-200 eV, soft-X-ray emission spectra of simple metals of Mg, Li, Al and Be were measured. Those intensity profiles correspond to partial density of states of valence electrons (bonding electrons) and also showed clear Fermi edges (top of the occupied state). At the Fermi edge of Mg-L emission (49.5 eV), an energy resolution was evaluated to be 0.16 eV. Si-L emission spectra of Si and TiSi₂ show a difference in those intensity distributions, indicating different valence-electron states for those materials. A comparison of B-K emission spectra of CaB₆ and LaB₆, which were obtained by using another grating of JS200N, is shown. A clear Fermi edge was also observed for LaB₆ at about 187 eV with an energy resolution of 0.4 eV.

Introduction

Recent tendency for miniaturizing semiconductor devices and developing new functional materials with nanometer scale size are eager for new evaluation methods not only for structural and elemental analyses but also for state analysis (physical properties) based on microscopy. Physical properties strongly depend on the electronic structure of valence electrons (bonding electrons). Thus, a high energy-resolution spectroscopy for valence electrons with a high spatial-resolution is extremely important to evaluate new functional materials. One promising way is an introduction of a valence-electron spectroscopy into electron microscopy.

Electron energy-loss spectroscopy (EELS) based on transmission electron microscopy (TEM) can obtain excitation spectra of valence electrons (transition “a” in Fig.1), which include information on dielectrics (refractive index, bandgap energy, interband transition

energies), from identified nanometer-scale specimen areas. The imaginary part of a dielectric function is proportional to the joint density of states of valence and conduction bands. Recent developments of monochromators for TEM enable us to examine physical properties in near infra-red energy region of nanoparticles [1] and also fine structures of partial density of states of conduction bands of nanometer scale specimen areas [2]. However, the density of states of valence electrons (bonding electrons) cannot be directly obtained by EELS.

For obtaining the density of states of valence electrons, soft-X-ray emission spectroscopy (SXES) instruments by using aberration corrected (varied-line-spaced) gratings have been introduced to transmission electron microscopes [3,4]. Especially, emissions due to electronic transitions from valence bands to an inner-shell level (transition “d” in Fig.1) are important. X-ray emissions due to transitions “c” in Fig.1, which is usually used for elemental analyses, do not have information on the density of states of valence bands. Combinations of SXES and EELS can figure out the total electronic structure from valence bands to conduction bands [3,5]. The energy resolutions of those SXES instruments

2-1-1 Katahira, Aoba-ku, Sendai 980-8577, Japan.

E-mail: terauchi@tagen.tohoku.ac.jp

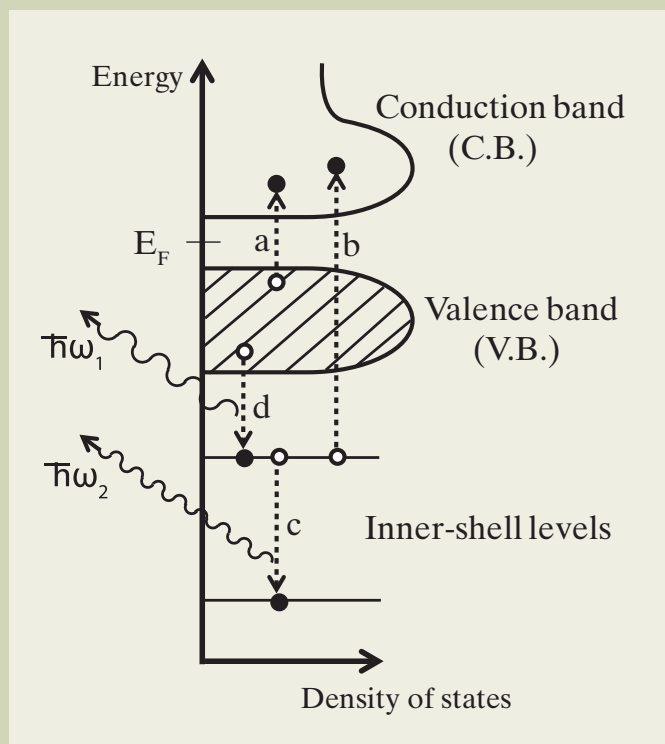


Fig. 1 Schematic diagram of electronic structure and electronic transitions relating to electron energy-loss spectroscopy (a and b) and X-ray emission spectroscopy (c and d). Soft-X-ray emission due to transition d gives us information on electronic states of valence electrons (bonding electrons).

are better than 1 eV for energies lower than 400 eV. This resolution is comparable to those of conventional X-ray photoelectron spectroscopy (XPS) or electron spectroscopy for chemical analysis (ESCA) instruments. The charging problem of a specimen in XPS/ESCA experiments, which causes a shift of a spectrum, does not come out in SXES experiments, because a soft-X-ray emission originates from an electronic transition inside a material. Furthermore, SXES instruments do not need an ultra-high vacuum condition due to a larger absorption length of soft-X-ray photons than a few tens nm. However, SXES method is inferior in detection efficiency compared to that of EELS due to a small efficiency of soft-X-ray emission and a small solid-angle for detection of spectrometers. Thus, an application of those SXES instruments to an electron probe microanalyzer (EPMA), which usually uses a much more beam current than that of a transmission electron microscope, overcomes the problem of pure S/N in soft-X-ray emission spectra obtained by transmission electron microscopes. This application will provide a valence electron spectroscopy method to examining an origin of a physical property with microscopy for a wide variety of materials developments.

In this report, results of a new SXES spectrometer attached to a transmission electron microscope are presented.

Instrumentation[6]

The present test SXES instrument has been designed to cover an energy region from 50 eV to 3800 eV by using four aberration-corrected (varied line-spaced; VLS) laminar-type gratings. This SXES spectrometer is based on flat-field grazing-incidence optics. Since a solid angle of this optics is small, it is

not so difficult to incorporate an SXES instrument with an electron microscope without any change in electron optics. A demerit of a small detection efficiency due to a small collection angle can be recovered by a few times using X-ray collection mirrors and dominantly by a high beam-current in case for EPMA/SEM.

Figure 2(a) shows a photo of the test SXES instrument attached to a transmission electron microscope of JEM-2010. This spectrometer is composed of a pair of X-ray collection mirrors, four VLS gratings and two detectors. The X-ray collection mirrors have gold surfaces and a length of 14 cm along the incoming X-ray path. Two VLS gratings (JS50XL and JS200N) among the four were used for present experiments. The upper detector in Fig.2(a), which is a CsI-coated two-stage multi-channel plate (MCP) optically coupled with a conventional front-illumination-type charge-coupled device (CCD) camera, is usually used for a lower energy region. An effective pixel size on MCP plane was evaluated to be 24 μm . Another detector (lower one) is a back-illuminated type CCD (direct CCD) without an anti-reflection coating with a pixel size of 12 μm . This smaller pixel sized detector has an advantage for obtaining high energy-resolution for a smaller energy-dispersion condition for higher energy X-rays.

A combination of a VLS grating of JS50XL, which covers from 50 eV to 200 eV, and the MCP+CCD detector was applied for measurements of Mg-L, Li-K, Al-L, Si-L and Be-K emissions. This grating has an Au-surface and an average groove density of 1200 lines/mm. The incident angle of X-ray is designed to be 86 degs. A solid angle for this combination with present X-ray collection mirrors was calculated to be 2.1 msr. The optics of this grating is shown in Fig.2(b).

The same one has already been applied to EPMA [7]. For B-K emission measurements, a VLS grating of JS200N, which covers from 150 eV to 350 eV, and the direct-CCD detector were applied. This second grating has a Ni-surface and an average groove density of 1200 lines/mm. The incident angle has been designed to be 87 degs, which is a little smaller than that of JS50XL.

In the following experiments, an accelerating voltage of the TEM was 100 kV. Beam size on

specimen area was varied from 0.6 μm to 5 μm to escape from irradiation damage. A parameter AQ ($\text{nA}\cdot\text{min}$), a beam current (nA) \times an acquisition time (min), is used for presenting acquisition conditions in this report.

Mg-L and Li-K emission spectra

Figure 3(a) shows a Li-K emission spectrum (V.B. \rightarrow K-shell) of Li and a Mg-L emission spectrum

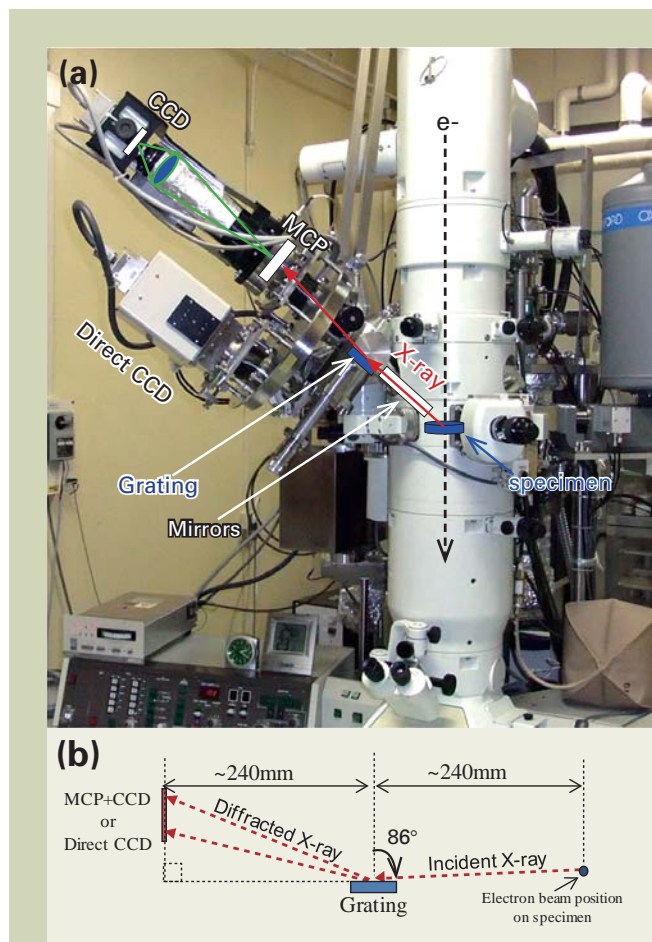


Fig. 2 (a) Photo of a newly constructed SXES instrument attached to a transmission electron microscope of JEM-2010. Upper detector is a multi-channel plate (MCP) optically coupled with a conventional front-illumination-type CCD camera. Lower one is a back-illuminated type CCD camera for direct detection of soft-X-ray. (b) A schematic figure of optics of the newly designed and manufactured grating of JS50XL for 50-200 eV.

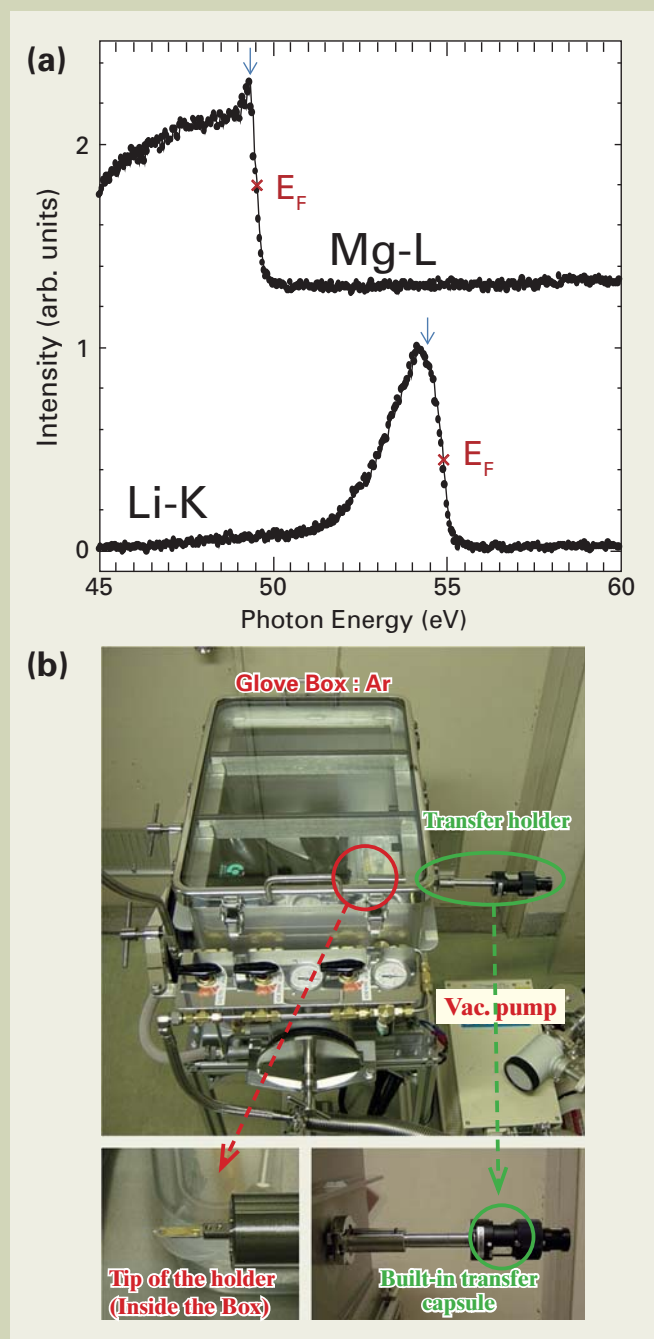


Fig. 3 (a) Mg-L emission spectrum (V.B. \rightarrow L-shell) of Mg-metal and Li-K emission spectrum (V.B. \rightarrow K-shell) of Li-metal. The energy resolution at E_F of the Mg-L emission spectrum was evaluated to be 0.16 eV. Core-hole effect in Li-K emission, suppression of intensity just below E_F , is seen. (b) A glove box and a specimen transfer holder, attached to the glove box, used for a preparation of Li-metal specimen.

(V.B.→L-shell) of Mg. AOs for Li-K and Mg-L were 950 nA·min and 400 nA·min, respectively. Since Li-metal is easily oxidized and/or nitrized in the air, a piece of Li-metal was mounted on a specimen transfer holder (JEOL-EM050611) attached to a glove box, and transferred to the SXES-TEM instrument. During the preparation and transfer processes, the specimen was kept under an Argon atmospheric condition. For this purpose, Ar gas was also used for the pre-pumping system of the transmission electron microscope. This transfer system is shown in Fig.3(b). A negligible hump at about 50 eV of Li-K emission may indicate little oxidization of metal surface during the specimen preparation.

Each spectrum shows a clear Fermi edge at the right-hand side end of each intensity distribution. A Fermi energy position (E_F), marked by x at the middle of each Fermi edge, corresponds to the top of the occupied energy level of each metal. The energy resolution at E_F of the Mg-L emission spectrum was evaluated to be 0.16 eV. Li-metal and Mg-metal are simple metals. Then, the electronic structure can be described by a free electron model. Thus, intensity distributions $I(E)$ of the lower part (apart from E_F) of those spectra are expected to be written as $I(E)_{Mg-L} \propto E^{1/2}$ (density of states of s -symmetry) and $I(E)_{Li-K} \propto E^{3/2}$ (density of states of p -symmetry) due to the dipole selection rule (the effect of transition matrix) [8]. E' is an energy measured from the bottom of V.B. An energy dependence of transition matrix elements, E^{-2} (E : photon energy), can be now omitted because an interested energy region is limited [8]. Experimental intensity distributions seem like those ways, indicating that the free electron model is appropriate for those metals.

Since Li has one valence electron per atom, the Fermi surface of a free electron model does not touch to Brillouin zone boundary. Thus, the intensity profile is expected to be simple as $I_{Li-K}(E') \propto E'^{3/2}$. However, it is clearly seen that the intensity just below E_F is apparently suppressed, indicated by an arrow, apart from $E'^{3/2}$. This discrepancy in Li-K emission has been explained by the effect of 1s core-hole, which exists

before an electronic transition from V.B. [9,10].

In case of Mg, which has two valence electrons per atom, the Fermi surface of a free electron model has some interaction with Brillouin zone boundary. The peak, observed just below E_F , indicated by an arrow, can be explained by the band-structure effect [11] and also the previous core-hole effect, which works to increase the intensity in case for L-emission [10].

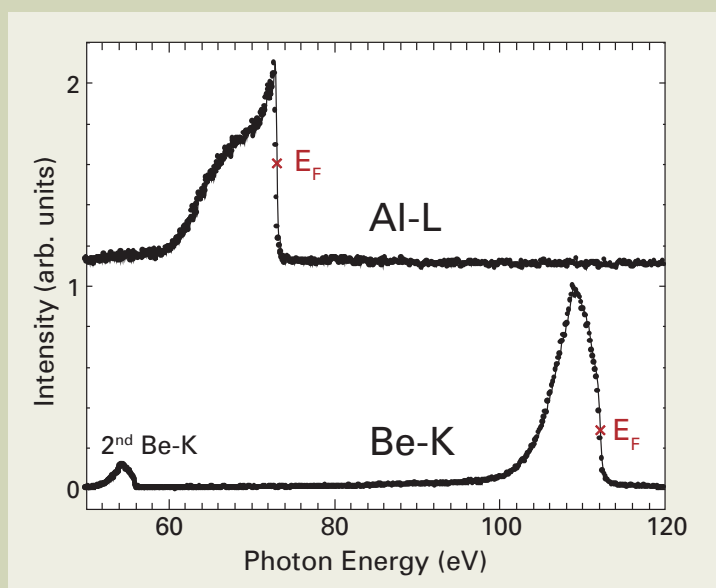
Al-L and Be-K emission spectra

Figure 4 shows an Al-L emission spectrum (V.B.→L-shell) of Al and a Be-K emission spectrum (V.B.→K-shell) of Be. AOs for Al-L and Be-K were 560 nA·min and 390 nA·min, respectively. In the Be-K emission spectra, a secondary diffracted intensity by the grating is also seen at a half of the energy of 1st order diffracted intensity at around 110 eV. Each spectrum shows a clear Fermi edge at the right-hand side end of each intensity distribution. A Fermi energy position, marked by x at the middle of each Fermi edge, corresponds to the top of the occupied energy level of each metal. The energy resolution at E_F of the Al-L emission spectrum was evaluated to be 0.2 eV.

Aluminum has three valence electrons per atom. Then, the Fermi sphere of a free electron model extends to higher Brillouin zones. Thus, intensity distribution is obeyed to $I(E') \propto E'^{1/2}$ in the lower part of V.B. as in the case of Mg-L emission and is affected by the band-structure in the upper part of V.B. The intense peak just below E_F has been explained by a presence of d -symmetry component [8].

Beryllium has two valence electrons per atom. Then, it can be expected a band-structure effect due to a larger free electron Fermi sphere than that of Li-metal. Thus, intensity distribution is obeyed to $I(E') \propto E'^{3/2}$ in the lower part of V.B. as in the case of Li-K emission and is strongly affected by the band-structure in the upper part of V.B. The delayed peak structure is well similar to a calculated density of states [12].

Fig. 4 Al-L emission spectrum (V.B.→L-shell) and Be-K emission spectrum (V.B.→K-shell). Each spectrum shows a clear Fermi edge. E_F position, marked by x at the middle of each Fermi edge, corresponds to the top of the occupied energy level of each metal. The energy resolution at E_F of the Al-L emission spectrum was evaluated to be 0.2 eV. Different characteristics in intensity profiles below E_F can be understood by the band-structure.



Si-L emission spectra

Figure 5 shows Si-L emission spectra (V.B.→L-shell) of Si and TiSi₂. AQs for Si and TiSi₂ were 150 nA·min and 300 nA·min, respectively. Due to the dipole selection rule, intensity distributions correspond to *s+d*-symmetry of the V.B. Since Si crystal is a semiconductor formed by covalent bonding of *sp*³ orbitals, intensity distribution of Si should correspond to *s*-symmetry part of V.B. It is seen that *s*-symmetry component contributes largely in the lower part and smaller in the upper part of V.B. Inversely, *p*-symmetry component possesses dominant part in the upper part and lesser in the lower part of V.B. [8]. The spectrum shows four structures as indicated by vertical lines. Those are assigned to special points of L₂, L₁, X₄ and L₃ in the band diagram [13].

TiSi₂ has been an interested conducting material in large-scale integrated circuit technology and a field-emission property of nanowires. Recently, Si/TiSi₂ heteronanostructures are attracting interest as a memory device [14] and an electrode material for energy storage [15]. Width of V.B. of TiSi₂ is almost the same with that of Si. The intense two peak structures, L₂ and L₁ in the lower part of V.B. of Si, may correspond to closely placed two peaks in TiSi₂. It is noted that the relative intensity in the upper part of V.B. (indicated by an arrow) is increased in TiSi₂ compared to that of Si. In a simple understanding for this change from Si seems a redistribution of *s*-symmetry component in V.B. of TiSi₂. However, this intensity increase is reported to be a contribution of *d*-symmetry of Si, which interacts with 3*d* orbitals of Ti, based on a theoretical calculation [16].

It is seen that energy positions of top of the V.B., indicated by a vertical broken line, is almost the same for both materials within experimental accuracy. The relative energy shift of TiSi₂ compared to Si can be evaluated by $\Delta E_B - E_g/2$ [8], where ΔE_B is a chemical shift value of Si-L level in TiSi₂ and E_g is an energy gap of 1.2 eV for Si. ΔE_B is reported to be about 0.5 eV [17]. Then, $\Delta E_B - E_g/2$ is calculated to be -0.1 eV, which is consistent with

present experimental results within the accuracy. A steep intensity increase at the top of V.B. in TiSi₂ should be attributed to a presence of the Fermi edge.

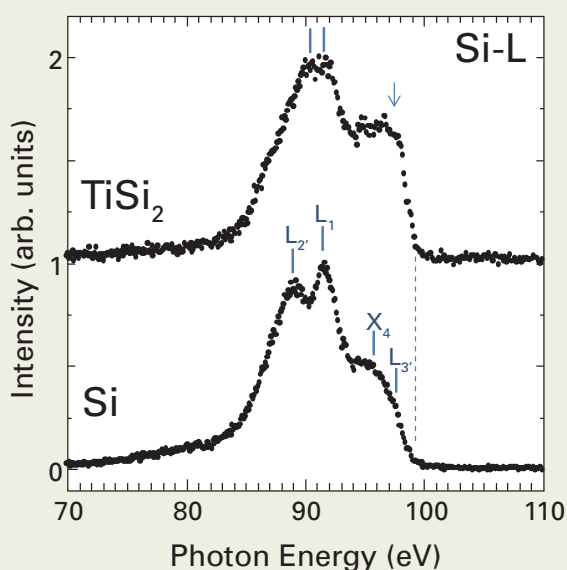
B-K emission spectra

Figure 6 shows B-K emission spectra (V.B.→K-shell) of CaB₆ (semiconductor) and LaB₆ (metal, well known cathode material). These intensity profiles have better signal to noise ratios compared to those to previous spectra. It is mainly due to a large AQ of 1560 nA·min for both spectra. Both materials belong to the same crystal structure of metal hexaborides MB₆. A schematic figure of the structure is shown as an inset. Due to the dipole selection rule, K-emission intensity corresponds to *p*-symmetry component in the V.B. Since boron atom has 2*s* and 2*p* valence electrons, intensity distribution of B-K emission should have larger intensity for the upper part of V.B. This situation is opposite compared to that in L-emission stated above.

The main peak in each spectrum is due to B-B bonding states between B atoms of B₆ cluster (intra-cluster orbitals), which are located at each corner of a cubic unit cell of the inset figure. The energy positions of the shoulder structures, indicated by vertical lines, are apparently different for the two materials. It may be due to a different B-B bonding length inside the cluster of the two materials [18]. The lower part of V.B. is assigned to inter-cluster bonding states labeled as B₆-B₆. CaB₆ shows a longer tail of B₆-B₆ intensity, which may be due to shorter inter-cluster distances causing larger energy dispersion for inter-cluster bonding states.

The most dominant difference between the two spectra is seen in the top part of the V.B. La and Ca atoms can transfer three and two electrons, respectively, to B₆-cluster network. Thus, higher energy levels should be occupied by electrons in LaB₆ than those in CaB₆. The spectrum of LaB₆ clearly shows an additional intensity at the right-hand side of the dominant B-B peak (top of V.B.) compared to that of CaB₆. It should be noted that a clear Fermi edge is seen corresponding

Fig. 5 Si-L emission spectra (V.B.→L-shell) of TiSi₂ and bulk silicon. Due to the dipole selection rule, intensity distributions correspond to *s+d*-symmetry of V.B. Intensity distribution shows that the *s*-symmetry is dominant in the lower part of V.B. Four structures labeled as L₂, L₁, X₄ and L₃ on the spectrum of Si correspond to special points in the band diagram.



to a metal nature of this material. The energy resolution at E_F was evaluated to be 0.4 eV. The Fermi level exists in a hybridized band of B-2p and La-5d orbitals [19].

Conclusion

A newly designed soft-X-ray spectrometer attached to a conventional transmission electron microscope has extended the detection lower limit from 60 eV to 50 eV by using a new VLS grating of JS50XL. This spectrometer enables us to detect Li-K emission from an identified specimen area by electron microscopy. Not only characteristic intensity distributions of K- and L-emissions of simple metals but also a core-hole effect in Li-K emission were observed. Structures in L-emission of Si were assigned to special points in the band diagram. The Fermi level in a cathode material of LaB_6 has been clearly observed. Thus, it is successfully shown that this SXES instrument provides a new valence electron spectroscopy method for chemical analyses not only for a wide variety of new functional materials developments but also for basic research of compounds.

Acknowledgments

The authors thank Mr. F. Sato for his skillful technical assistance. This development was conducted as one project of Collaborative Development of Innovative Seeds (Practicability verification stage) by Japan Science and Technology Agency. Measurements of Li-K emission were partly supported by a Grant-in-Aid for Scientific Research on Priority Areas 'New Materials Science Using Regulated Nano Spaces-Strategy in Ubiquitous Elements' by the Ministry of Education, Culture, Sports, Science and Technology of Japan (No.19051002).

References

[1] Y. Sato, M. Terauchi, M. Mukai, T. Kaneyama and K. Adachi, *Ultramicroscopy*, **111**, 1381 (2011).

- [2] Y. Sato, M. Terauchi, W. Inami and A. Yoshiasa, *Diamond and Related Materials*, **25**, 40 (2012).
- [3] M. Terauchi and M. Kawana, *Ultramicroscopy*, **106**, 1069 (2006).
- [4] M. Terauchi, M. Koike, K. Fukushima and A. Kimura, *Journal of Electron Microscopy*, **59**, 251 (2010).
- [5] M. Terauchi, *Microscopy Research and Technique*, **69**, 531 (2006).
- [6] M. Terauchi, H. Takahashi, N. Handa, T. Murano, M. Koike, T. Kawachi, T. Imazono, M. Koeda, T. Nagano, H. Sasai, Y. Oue, Z. Yonezawa and S. Kuramoto, *Journal of Electron Microscopy*, **61**, 1 (2012).
- [7] H. Takahashi, N. Handa, T. Murano, M. Terauchi, M. Koike, T. Kawachi, T. Imazono, M. Koeda, T. Nagano, H. Sasai, Y. Oue, Z. Yonezawa and S. Kuramoto, *Microscopy & Microanalysis*, **16(suppl.2)**, 34 (2010).
- [8] D.J. Fabian, L.M. Watson and C.A.W. Marshall, *Rep. Prog. Phys.*, **34**, 601 (1972).
- [9] F.K. Allotey, *Phys. Rev.*, **157**, 467 (1967).
- [10] Y. Mizuno and K. Ishikawa, *J. Phys. Soc. Japan*, **25**, 627 (1968).
- [11] R.P. Gupta and A.J. Freeman, *Phys. Rev. Lett.*, **36**, 1194 (1976).
- [12] S.T. Inoue and J. Yamashita, *J. Phys. Soc. Japan*, **35**, 677 (1973).
- [13] S. Shin, A. Agui, M. Watanabe, M. Fujisawa, Y. Tezuka and T. Ishii, *Phys. Rev. B*, **53**, 15660 (1996).
- [14] Y. Zhu, B. Li and J. Liu, *J. Appl. Phys.*, **101**, 063702 (2007).
- [15] S. Zhou, X. Liu and D. Wang, *Nano Lett.*, **10**, 860 (2010).
- [16] P.J.W. Weijs, H. van Leuken, R.A. de Groot and J.C. Fuggle, *Phys. Rev. B*, **44**, 8195 (1991).
- [17] Y. Yamauchi, M. Yoshitake and SERD project group of SASJ, *J. Surface Analysis*, **9**, 432 (2002).
- [18] "The chemistry of Boron and its Compounds", ed. by E.L. Muetterties, John Wiley & Sons, Inc., New York (1967), p.119.
- [19] S. Kimura, H. Harima, T. Nanba, S. Kunii and T. Kasuya, *J. Phys. Soc. Japan*, **60**, 745 (1991).

Fig. 6 B-K emission spectra of CaB_6 and LaB_6 . Due to the dipole selection rule, intensity distributions correspond to p -symmetry of V.B. Intensity distribution shows that the p -symmetry is dominant in the upper part of V.B. The most dominant difference between the two spectra is seen in the top part of V.B. The spectrum of LaB_6 clearly shows a Fermi edge corresponding to a metal nature of the material. The energy resolution at E_F was evaluated to be 0.4 eV.

